

# Performance prediction of a solar district cooling system in Riyadh, Saudi Arabia – A case study

G. Franchini\*, G. Brumana, A. Perdichizzi

Department of Engineering and Applied Sciences, University of Bergamo, 5 Marconi Street, Dalmine 24044, Italy

## ARTICLE INFO

### Keywords:

Solar cooling  
District cooling  
Parabolic trough  
Absorption chiller  
Thermal storage

## ABSTRACT

The present paper aims to evaluate the performance of a solar district cooling system in typical Middle East climate conditions. A centralized cooling station is supposed to distribute chilled water for a residential compound through a piping network. Two different solar cooling technologies are compared: two-stage lithium-bromide absorption chiller (2sABS) driven by Parabolic Trough Collectors (PTCs) vs. single-stage lithium-bromide absorption chiller (1sABS) fed by Evacuated Tube Collectors (ETCs). A computer code has been developed in Trnsys® (the transient simulation software developed by the University of Wisconsin) to simulate on hourly basis the annual operation of the solar cooling system, including building thermal load calculation, thermal losses in pipes and control strategy of the energy storage. A solar fraction of 70% was considered to size the solar field aperture area and the chiller capacity, within a multi-variable optimization process. An auxiliary compression chiller is supposed to cover the peak loads and to be used as backup unit. The two different solar cooling plants exhibit strongly different performance. For each plant configuration, the model determined the optimal size of every component leading to the primary cost minimization. The solar district cooling configuration based on 2sABS and PTCs shows higher performance at Riyadh (KSA) climate conditions and the overall cost is 30% lower than the one of the single-stage absorption chiller plant.

## 1. Introduction

District energy systems have attracted great interest over the last decades thanks to the undeniable environmental and economic benefits and the high level of efficiency and reliability. Boran et al. [1] examined district heating systems and concluded that they are responsible for 33% equivalent CO<sub>2</sub> savings compared to conventional gas boilers used for heating, and electricity from the grid for electrical demand. Casisi et al. [2] investigated a distributed cogeneration system with a district heating network, applied to a real city center: they demonstrated that both microturbines and ICEs designed for CHP applications are competitive with respect to conventional energy supply. Many papers focus on improving the system at the network level. The network operation is deeply analyzed in [3,4]: the authors developed a detailed numerical model based on a quasi-static approach for the hydraulic behavior and a transient model for the thermal one. Despite most of the existing district energy systems are for heating purpose [5], in recent years the development of district cooling systems has grown up due to the increase of the global energy demand for air conditioning. The growth of district cooling systems is linked to the development and marketing of absorption chillers: Ameri and Besharati [6] evaluated

different integration scenarios including cogeneration, trigeneration and district heating/cooling.

A further milestone in the development of district energy systems has been derived from the integration of energy storages in district heating [7–9], as well as in district cooling. The storage can be diurnal or seasonal [10]. Powell et al. [11] presented a new methodology to optimize the operation of the cooling unit coupled with tanks. Gang et al. [12] investigated a district cooling system with thermal storage integrated into a trigeneration plant serving a residential compound in a subtropical area. The results of their work show that an appropriate design can lead to economic, environmental and energy savings.

The integration of renewable sources into district energy systems is a way to increase the environmental sustainability, in spite of the impact on the initial investment [8]. Liew et al. [13] analyzed several options to integrate different energy systems including renewable in different types of building complexes. The exploitation of geothermal energy for district heating systems has been deeply investigated [14]. Heat can be extracted from the ground directly or with the use of heat pumps [15].

Integrating solar energy into district heating systems is a challenge of recent years [16]. The main issues are the variability of the source,

\* Corresponding author.

E-mail address: [giuseppe.franchini@unibg.it](mailto:giuseppe.franchini@unibg.it) (G. Franchini).

**Nomenclature**

<i>1sABS</i>	single-stage absorption chiller	<i>E<sub>coll</sub></i>	heat collected by the solar field (MWh)
<i>2sABS</i>	two-stage absorption chiller	<i>E<sub>rad</sub></i>	radiant solar energy (MWh)
<i>a<sub>0</sub></i>	collector optical efficiency	<i>ETC</i>	evacuated tube collector
<i>a<sub>1</sub></i>	collector 1st order loss coefficient (W/m <sup>2</sup> /K)	<i>G<sub>-value,w</sub></i>	window solar factor
<i>a<sub>2</sub></i>	collector 2nd order loss coefficient (W/m <sup>2</sup> /K <sup>2</sup> )	<i>GHI</i>	global horizontal irradiance (W/m <sup>2</sup> )
<i>A<sub>coll</sub></i>	aperture area of the solar field (m <sup>2</sup> )	<i>HX</i>	heat exchanger
<i>AHU</i>	air handling unit	<i>ICE</i>	internal combustion engine
<i>BTI</i>	beam tilted irradiance (W/m <sup>2</sup> )	<i>PTC</i>	parabolic trough collector
<i>Cap<sub>Abs</sub></i>	capacity of the absorption chiller (kW)	<i>Q<sub>abs</sub></i>	cooling power of absorption chiller (1s or 2s) (kW)
<i>CC</i>	compression chiller	<i>Q<sub>aux</sub></i>	cooling power of auxiliary chiller (kW)
<i>CHP</i>	combined heat and power	<i>Q<sub>coll</sub></i>	thermal power collected by solar field (kW)
<i>CHW</i>	chilled water	<i>Q<sub>rad</sub></i>	radiant power (kW)
<i>Cost<sub>Abs</sub></i>	unit cost of the absorption chiller (\$/kW)	<i>SF</i>	solar fraction
<i>Cost<sub>coll</sub></i>	unit cost of solar collectors (\$/m <sup>2</sup> )	<i>T</i>	mean temperature between inlet and outlet flow rates (°C)
<i>Cost<sub>tank</sub></i>	unit cost of the tank (\$/m <sup>3</sup> )	<i>T<sub>amb</sub></i>	ambient temperature (°C)
<i>CR</i>	concentration ratio	<i>T<sub>tank.bottom</sub></i>	temperature at tank bottom (°C)
<i>CW</i>	cooling water	<i>T<sub>tank.top</sub></i>	temperature at tank top (°C)
<i>DNI</i>	direct normal irradiance (W/m <sup>2</sup> )	<i>U<sub>roof</sub></i>	roof U-value (W/m <sup>2</sup> /K)
<i>E<sub>abs</sub></i>	cooling energy produced by the absorption (1s or 2s) chiller (MWh)	<i>U<sub>-value,w</sub></i>	window U-value (W/m <sup>2</sup> /K)
<i>E<sub>aux</sub></i>	cooling energy produced by the auxiliary chiller (MWh)	<i>U<sub>wall</sub></i>	wall U-value (W/m <sup>2</sup> /K)
		<i>Vol<sub>tank</sub></i>	tank volume (m <sup>3</sup> )
		<i>η</i>	efficiency (–)
		<i>θ</i>	incidence angle (°)

thus requiring a thermal energy storage system, and the critical overheating during the off-heating season. To avoid these problems keeping high the solar contribution, it is essential to design powerful predictive models of load management and storage tanks: Daniel Trier [17] has investigated district heating systems with a solar fraction of more than 70%. Often, the solar thermal systems operating in a district heating network are coupled with biomass boilers [18]. Therefore, research is focused on improving the efficiency of the production plant [19] and the network [20,21], by means of detailed computer models and simulation tools [22] and genetic optimization algorithms [23]. Subsequently, the integration of the solar contribution is also extended to the cooling systems as a direct result of the development of solar cooling technologies for individual buildings [24].

Only a few articles deal with the integration of solar energy in district cooling systems [25–28]. Marugán-Cruz et al. analyzed the integration of a high temperature solar technology (solar tower) into a district cooling system to enhance the energy surplus in the warm season [29]. The integration of concentrated solar power plants with cooling energy production is investigated also in [30], where the authors demonstrated that the combined power and cooling production for plants operating in island-mode can improve the overall global efficiency. The abovementioned systems are basically large-scale solar power plants with heat recovery for cooling production via absorption or adsorption chillers. For smaller sizes, typically the solar field is directly connected to the thermally driven chiller [31–33]. The most common configuration is based on *ETCs* coupled with a single-stage LiBr absorption chiller [34,35]: evacuated tube collectors with selective surface exhibit efficiency higher than 65% for a fluid temperature in the range 85–100 °C, typical for the generator of *1sABS*. A higher overall efficiency is expected from solar cooling systems based on two-stage absorption chillers, whose *COP* is usually around 1.3–1.4. Such units require a supply temperature higher than 150 °C [36]. For these temperature levels, the best solar field option is a medium concentration collector like a *PTC*. Although parabolic troughs can exploit only the beam radiation, the reduction of the heat loss area permits to keep high the efficiency for relatively high fluid temperatures (up to 200 °C). Mazloumi et al. [37] investigated the operation of *PTCs* in a small-scale solar cooling system: they documented a collector efficiency higher than 68% when coupled to a *1sABS*. El Fadar et al. [38] presented a numerical study related to a continuous adsorption refrigeration system

powered by parabolic trough solar collectors, with operating temperatures varying in the range 20–160 °C.

In the open literature, the potential benefits deriving from the integration of *PTCs* and *2sABS* are substantially unexplored. Starting from previous researches on the modeling and the analysis of buildings and solar cooling plants [39,40], this work presents a solar district cooling model capable of predicting with accuracy the global performance of the system and the behavior of each single component in design and off-design operating conditions.

Moreover, the paper deals with the system optimization. It is well known that an optimal plant configuration is crucial for solar driven technologies, in order to maximize the overall efficiency and to minimize the investment costs, as well documented by Hang et al. [41]. Among the available optimization methods, the integration of dynamic simulations based on the Trnsys software and the Hooke and Jeeves optimization algorithm [42] was proved to be a remarkable solution. A deep explanation of the Hooke and Jeeves direct search algorithm and its benefits is reported by Kirgat and Surde in [43].

The paper firstly introduces the Trnsys models developed for reproducing the cooling load of a residential compound, the district cooling network and the cooling plant based on two different absorption chillers: double-stage unit powered by a *PTC* field and single-stage machine driven by *ETCs*. A set of dynamic simulations have been performed using the GenOpt optimization tool in order to maximize the thermo-economic performance of the systems.

## 2. Model description

### 2.1. Building model

The case study is based on a residential compound in Saudi Arabia. The current governmental vision encourages for the development of new residential districts based on energy-efficient buildings and solar-driven technologies. The compound is supposed to be composed by 96 single-family houses. Each building is a two-floor villa with total surface 575 m<sup>2</sup> and global volume 1725 m<sup>3</sup>. The building architecture reproduces the standard residential building style in Saudi Arabia. The 3D software Google Sketch Up coupled with the plug-in Trnsys3D was used to model the building geometry. The building model allows for evaluating the shading effects and the radiation on walls and windows. Fig. 1



Fig. 1. Residential compound.

shows a rendering of the residential compound.

The geometrical model was imported in a Trnsys deck based on the Multizone Building Type to calculate the cooling load over 1-year period on hourly basis. The meteorological conditions were derived from the Meteoronorm international database [44]: a detailed description of the ambient conditions is provided in the Section 3.1. Internal loads due to appliances, lights and occupancy were evaluated for each room and considered in the calculation. The variability of internal loads have been taken into account according to the building occupancy. The envelope characteristics comply with the Dubai Green-Building Regulation and Specification (the reference standard for new constructions in all the Gulf region) and include all the parameters considered for the development of the energy model. The Trnsys model performs a detailed dynamic simulation able to calculate the cooling load of each room on hourly basis. The main parameters related to the internal loads together with the thermal characteristics of the envelope are listed in Table 1.

## 2.2. District cooling network

The district piping network was conceived to meet the cooling demand of the compound made of 96 detached homes. The complex is divided into 4 sub-district of 24 houses fed by different ramifications delivering the chilled water to the villas. The overall length of the distribution network is 16.8 km. A conceptual diagram is shown in Fig. 2. The solar field is supposed located in a dedicated area close to the central cooling station. Losses in the piping connecting the solar field to the absorption chiller were considered negligible.

The network is designed for a maximum speed of 2.75 m/s in the main branches and 2 m/s in the smaller branches. The tube insulation thickness is 2 in.; all pipeline parameters are summarized in Table 2 and represent the characteristics of commercial products [45]. Chasapis et al. reported in [18] an optimization of the working parameters of a district network: in the present analysis, those optimal values have been considered. Moreover, such values - including the water velocity - are consistent with the best practices for network design suggested by the Engineering Association and the pipe manufacturers [46].

The control strategy of the heat transfer substations is based on a mass flow modulation. The nominal temperature difference across the heat exchangers is equal to 7 °C. The actual delta T between supply and return line at the pumping station allows for determining the heat loss along the network.

## 2.3. Solar field and chiller

The cooling load generated by the compound is assumed to be covered for a percentage by a solar cooling system. Two different configurations are analyzed and compared: *PTC* with *2sABS* vs. *ETC* with *1sABS*. The latter is the typical system of most applications at commercial stage. The former is the advanced configuration proposed in the present work.

For both plant configurations, the solar field aperture area, the hot storage tank volume and the chiller cooling capacity have been optimized through the software GenOpt interacting with Trnsys. GenOpt is a tool for multidimensional optimization of an objective function computed by a simulation program [47]; the Hooke and Jeeves algorithm is the optimization method selected for the cases investigated in the present study. This method searches the optimal solution in a specific range (Constrained Optimization) in the presence of continuous and discrete constraints on the operation parameters and on the technical data of the plant components. On the base of annual Trnsys simulations, GenOpt determines the optimal values for the variables, minimizing the budget cost and, at the same time, complying with the solar fraction target according to the Hooke and Jeeves direct search method. Solar fraction (*SF*) is the percentage of cooling load covered by the solar cooling plant: the residual fraction is supposed satisfied by conventional electric chillers. Typically, solar driven absorption chiller are sized to fulfill the base load, leaving the peak loads to a backup system. For the present study a *SF* = 0.70 has been considered.

Fig. 3 shows how the computer codes interact with each other. A Trnsys building model provides the cooling load for each villa. The network model calculates the cumulative cooling energy demand, including pipe losses. The Trnsys model of the solar cooling plant simulates the operation over 1-year period and calculates the annual solar

Table 1  
Building envelope characteristics.

Comfort & Gains			Wall layers & Windows		
Temperature set point	°C	24	$U_{wall}$	$W/m^2/K$	0.57
Relative humidity set point	%	50	Wall thickness	m	0.27
Air changes	Vol/h	0.60	Wall solar absorptance	%/100	0.30
Recuperative HX efficiency	%	60	$U_{roof}$	$W/m^2/K$	0.30
Infiltration	Vol/h	0.4	Roof thickness	m	0.27
Lighting (peak)	$W/m^2$	19	Roof solar absorptance	%/100	0.20
Internal gains (peak)	kW	3	$U_{value,w}$	$W/m^2/K$	1.9
Occupancy (average - max)	Nr.	4–10	$G_{value,w}$	%/100	0.621

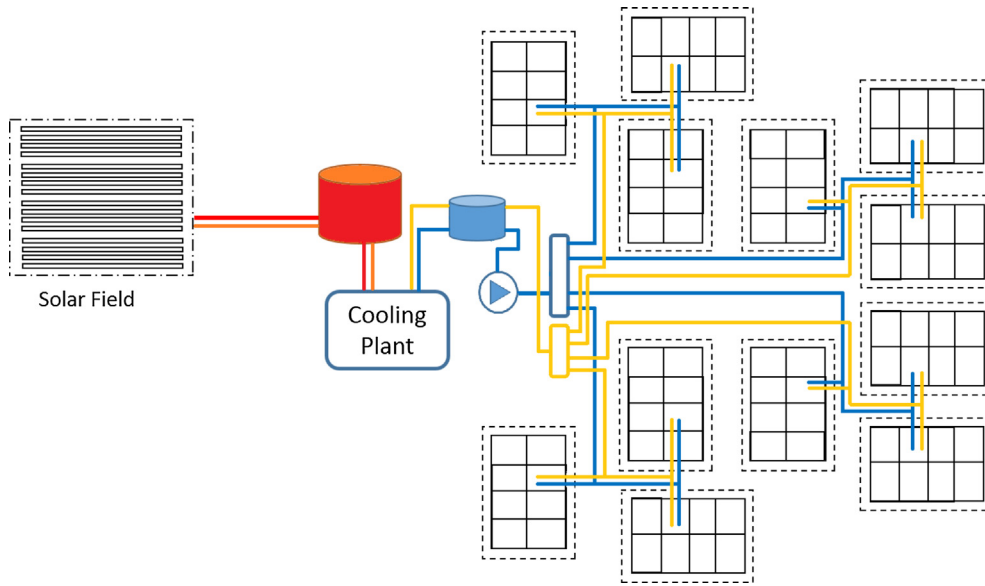


Fig. 2. District cooling network.

Table 2  
Pipeline parameters.

D (m)	Insulation thickness (inch)	Length (m)	Linear heat loss (W/m)	Surface per unit length (m <sup>2</sup> /m)	Heat loss coefficient (W/m <sup>2</sup> /K)
0.08	2.00	7200	0.7925	0.2513	1.2218
0.10	2.00	4800	0.8839	0.3142	1.0903
0.12	2.00	4800	0.9754	0.3770	1.0026

fraction. GenOpt changes the value of the optimization variables from a minimum to a maximum: the set of parameters is entered to Trnsys, which performs the annual simulation.

The objective function is the budget cost of the solar cooling system (solar field, tank and chiller). Table 3 reports the unit costs considered for the present investigation. The unit cost of the components was provided by the manufacturers (absorption chillers and compression chiller) or derived from published reports [48,49].

The objective function is reported in Eq. (1): the optimization involves collector area, tank volume and chiller capacity, whose values are multiplied by their unit costs (Table 3). A penalty coefficient allows for neglecting the solutions that do not comply with the desired solar fraction.

Table 3  
Budget unit costs.

<b>Collectors</b>		
Evacuated Tube Collectors	\$/m <sup>2</sup>	500
Parabolic Trough Collectors	\$/m <sup>2</sup>	480
<b>Storage</b>		
Pressurized Hot Water Tank (2sABS)	\$/m <sup>3</sup>	1050
Hot Water Tank (1sABS)	\$/m <sup>3</sup>	450
<b>Chiller</b>		
1s Absorption Chiller	\$/kW	400
2s Absorption Chiller	\$/kW	560

The optimization parameters (minimum and maximum value, re-search step) are shown in Table 4 with the optimized results. The optimization process is based on the Hooke and Jeeves pattern search method: starting from an initial variable combination, the algorithm evaluates the objective function by changing each variable value in both directions. The configuration is optimized in a two-step process. The first step searches for the combination meeting the desired solar fraction. The second step searches for the combination minimizing the total cost.

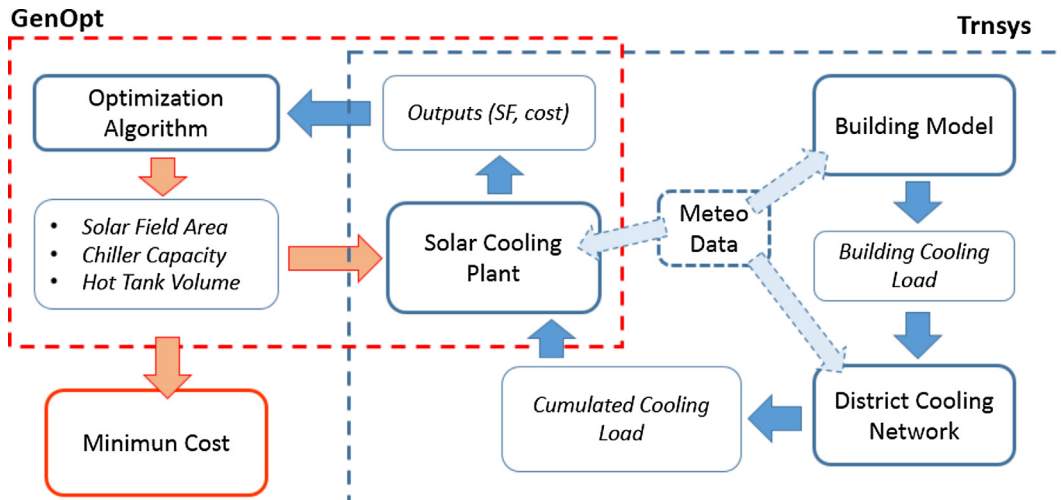


Fig. 3. Simulation and optimization algorithm.



**Table 4**  
Optimization parameters.

Collectors Area		2sABS	1sABS
Minimum value	m <sup>2</sup>	8000	12,000
Maximum value	m <sup>2</sup>	16,000	22,000
Step	m <sup>2</sup>	500	500
Optimum Value	m <sup>2</sup>	9035	15,600
Storage			
Minimum value	m <sup>3</sup>	300	600
Maximum value	m <sup>3</sup>	800	1400
Step	m <sup>3</sup>	50	50
Optimum Value	m <sup>3</sup>	400	995
Chiller			
Minimum value	kW	1800	1800
Maximum value	kW	3000	4000
Step	kW	200	200
Optimum Value	kW	2315	3250
Minimum cost function value	Mio USD	6.053	9.550

**Table 5**  
PTC-2sABS cooling plant characteristics.

Solar Field (PTC)			2s Absorption Chiller (Commercial)		
Total aperture area	m <sup>2</sup>	9035	Nominal Capacity <sup>a</sup>	kW	2315
Outlet set point temperature	°C	170	Rated COP <sup>a</sup>	–	1.39
CR	–	60	Hot source range	°C	121–175
Optical efficiency (a <sub>0</sub> )	–	0.7719	Storage		
1st order heat loss coeff. (a <sub>1</sub> )	W/m <sup>2</sup> /K	0.1803	Hot tank volume	m <sup>3</sup>	400
2nd order heat loss coeff. (a <sub>2</sub> )a <sub>2</sub>	W/m <sup>2</sup> /K <sup>2</sup>	0.0258	Cold tank volume	m <sup>3</sup>	200

<sup>a</sup> Chilled water (in-out) 12–7 °C; hot water (in-out) 175–155 °C; cooling water (in-out) 30–35 °C.

**Table 6**  
ETC-1sABS cooling plant characteristics.

Solar Field (ETC)			Single-stage Absorption Chiller (Commercial)		
Total aperture area	m <sup>2</sup>	15,600	Nominal Capacity <sup>a</sup>	kW	3250
Outlet set point temperature	°C	94	Rated COP <sup>a</sup>	–	0.723
CR	–	1	Hot source range	°C	65–95
Optical efficiency (a <sub>0</sub> )	–	0.718	Storages		
1st order heat loss coeff. (a <sub>1</sub> )	W/m <sup>2</sup> /K	0.974	Hot tank volume	m <sup>3</sup>	995
2nd order heat loss coeff. (a <sub>2</sub> )a <sub>2</sub>	W/m <sup>2</sup> /K <sup>2</sup>	0.005	Cold tank volume	m <sup>3</sup>	200

<sup>a</sup> Chilled water (in-out) 12–7 °C; hot water (in-out) 90–80 °C; cooling water (in-out) 30–35 °C.

$$f_{\min} = A_{\text{Col}} \cdot \text{Cost}_{\text{Col}} + Cap_{\text{Abs}} \cdot \text{Cost}_{\text{Abs}} + Vol_{\text{tank}} \cdot \text{Cost}_{\text{tank}} + \text{Penalty}_{(\text{SF} < 0.70)} \quad (1)$$

### 2.3.1. PTC-2sABS

In the present solar cooling plant configuration the solar field is based on Parabolic Trough Collectors supplying pressurized water to a hot storage tank. A variable speed pump regulates the mass flow rate to keep the temperature level at the set point (170 °C). The PTC field is Nord-South oriented and equipped with 1-axis tracking device. The field efficiency is computed according with the quadratic Eq. (2); the loss coefficients are kept from the data sheet of a commercial trough and are reported in Table 5.

$$\eta = a_0 - a_1 \frac{\bar{T} - T_{\text{amb}}}{BTI \cdot CR} - a_2 \frac{(\bar{T} - T_{\text{amb}})^2}{BTI \cdot CR} \quad (2)$$

The thermal efficiency  $\eta$  is defined according to ASHRAE (93/2003) standard and rated by SRCC. The parameters  $a_0$ ,  $a_1$  and  $a_2$  are respectively the optical efficiency, the first order loss coefficient and the second order loss coefficient: their values are reported in Table 5 for PTCs and Table 6 for ETCs. Because of the 1-axis tracking system, the troughs do not collect the DNI, but the beam tilted irradiance, defined as follows:

$$BTI = DNI \cdot \cos(\theta) \quad (3)$$

The hot water pumped from the storage is delivered to a two-stage lithium-bromide absorption chiller. The model includes the efficiency maps provided by a chiller manufacturer and reported in Fig. 4. The left part of the Fig. 4 shows the capacity reduction (fraction of the nominal capacity) for different cooling water temperatures and chilled water temperatures. The right part shows the thermal input required by the chiller operating at part load (with different cooling water temperatures) as a fraction of the design heat input. The optimal cooling capacity determined by GenOpt resulted to be 2315 kW. The chiller operates in on-off mode (at the design load) and feeds a cold storage tank of 200 m<sup>3</sup>. The actual chiller COP is affected by the temperature levels of the external circuits (hot water, chilled water and cooling water) and it is computed and updated at each time step. The main operating parameters (in design conditions) and the optimal values computed by GenOpt are reported in Table 5.

The heat rejection system is based on a cooling tower; the control system adapts the fan speed to keep the cooling water temperature in the range 25–30 °C.

A proactive control strategy has been implemented. When the temperature in the buffer tank located between the chiller and the district network rises up to 10 °C, the two-stage absorption chiller is switched on until the level of 5 °C is achieved. An auxiliary chiller contributes to cool down the cold storage tank if the cooling power provided by the absorption chiller is not sufficient to satisfy the load. The auxiliary chiller is designed to cover the peak cooling load in the event of a system failure due to lack of radiation or depletion of thermal storage. The control system switches off the absorption chiller to avoid crystallization problems when the hot water from the solar field and the cooling circuit reach the lower (121 °C) and upper (35 °C) temperature limits respectively.

The Trnsys deck for the PTC-2sABS plant configuration is shown in Fig. 5. Some ‘types’ (this is the name of the Trnsys routines) are from the software database and TESS libraries, while other components are based on proprietary models, developed by the authors. The type ‘Meteo’ reads the file of the Meteonom database, providing solar radiation on tilted surfaces, ambient temperature and relative humidity. The solar loop, including the collector field and the pressurized hot water tank, is highlighted with the bold red line. The thermal storage is linked (orange line) to the absorption chiller, which supplies chilled water to the cold tank (light blue line). The type ‘ThermalLoad’ reads an external file containing the required cooling load on hourly basis. The green line depicts the cooling circuit connected to the evaporative cooling tower.

### 2.3.2. ETC-1sABS

As mentioned before, the most common solar cooling configuration is based on a single-stage lithium-bromide absorption chiller driven by Evacuated Tube Collectors. The cooling plant configuration is similar to the one described in the previous paragraph, but with different settings and different sizes. Table 6 reports the optimized parameters related to the solar field and the chiller, while Fig. 6 shows the 1sABS performance curves for different inlet cooling water (CW) temperatures.

It can be noted that all the optimized variables (aperture area, chiller capacity, hot tank volume) exhibit higher values, compared to

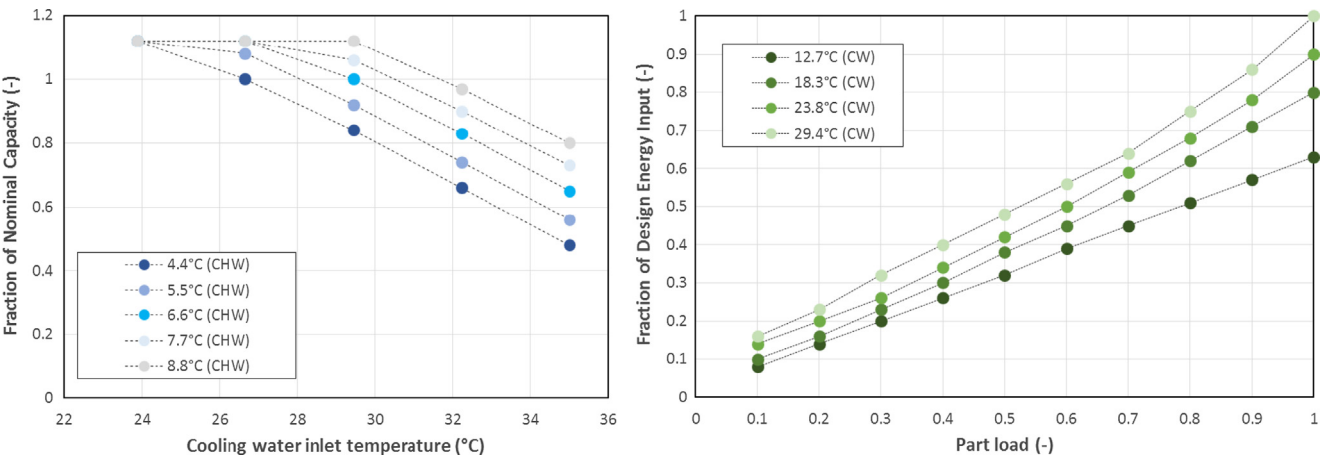


Fig. 4. Two-stage absorption chiller performance maps.

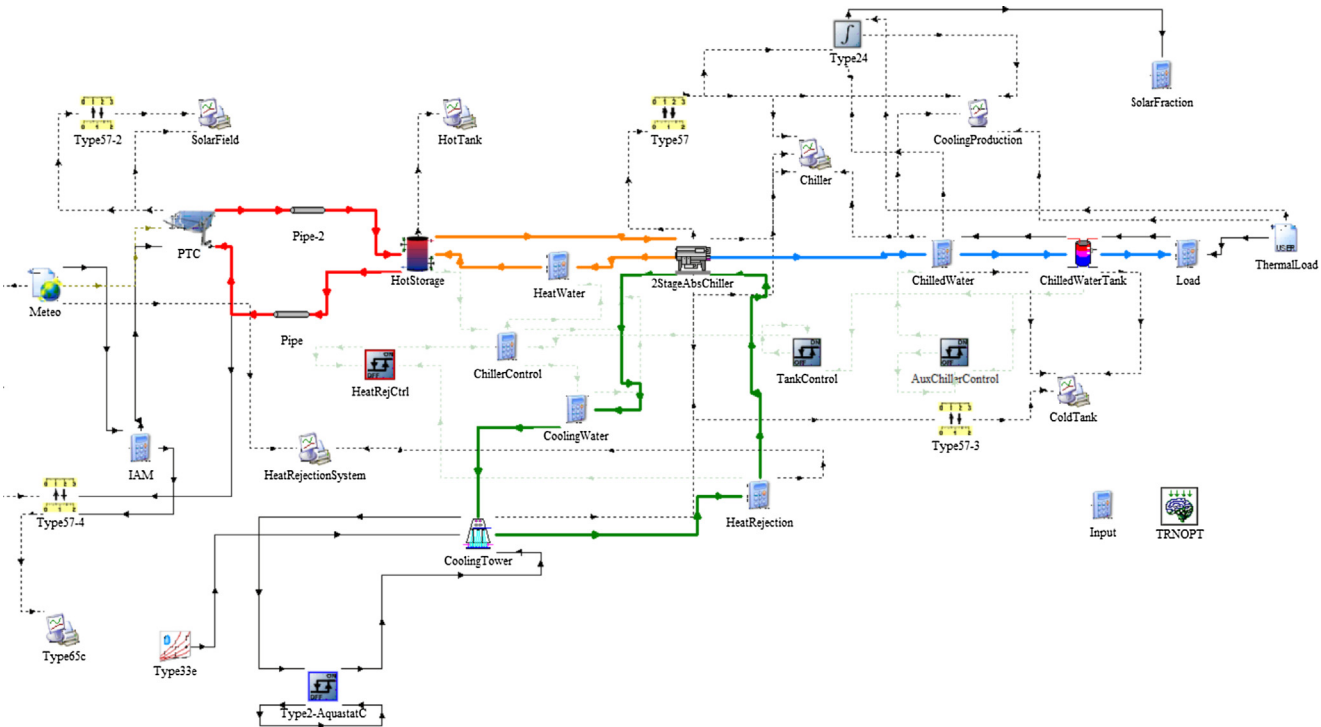


Fig. 5. Trnsys deck of the solar cooling plant configuration PTC-2sABS.

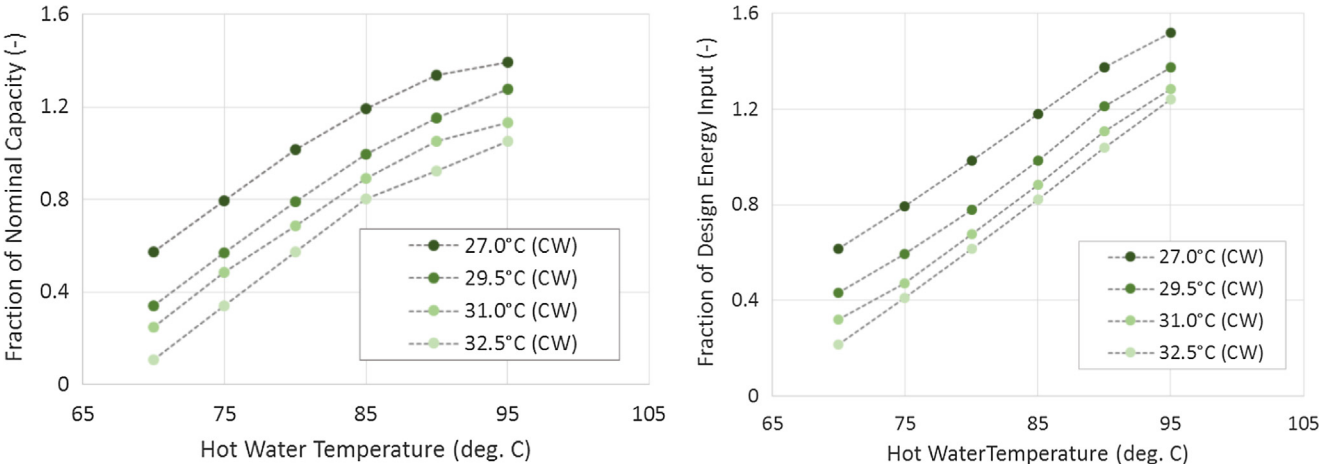


Fig. 6. Single-stage absorption chiller performance maps.

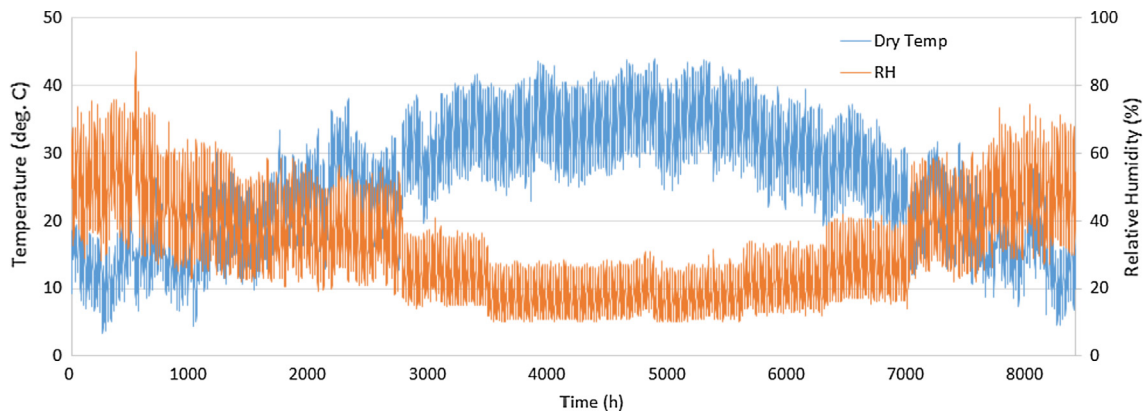


Fig. 7. Ambient temperature and relative humidity.

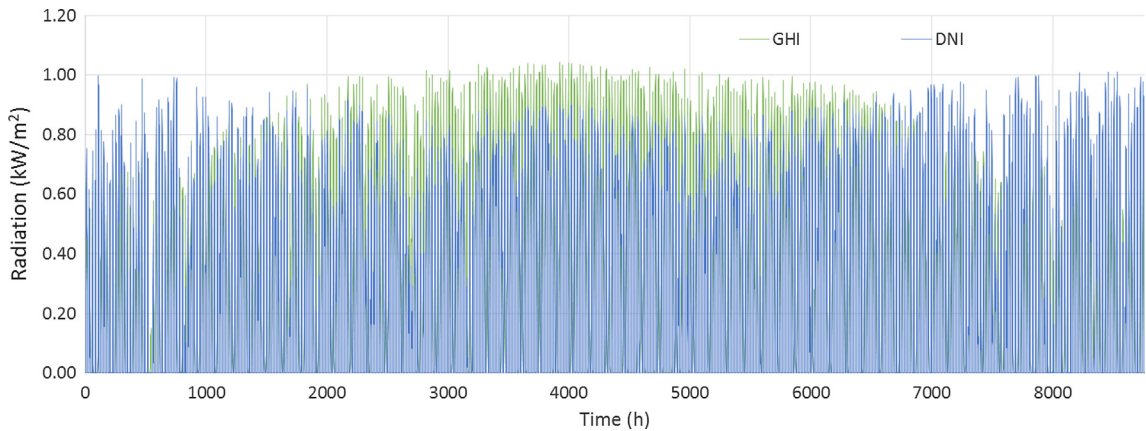


Fig. 8. Global horizontal irradiance vs. direct normal irradiance.

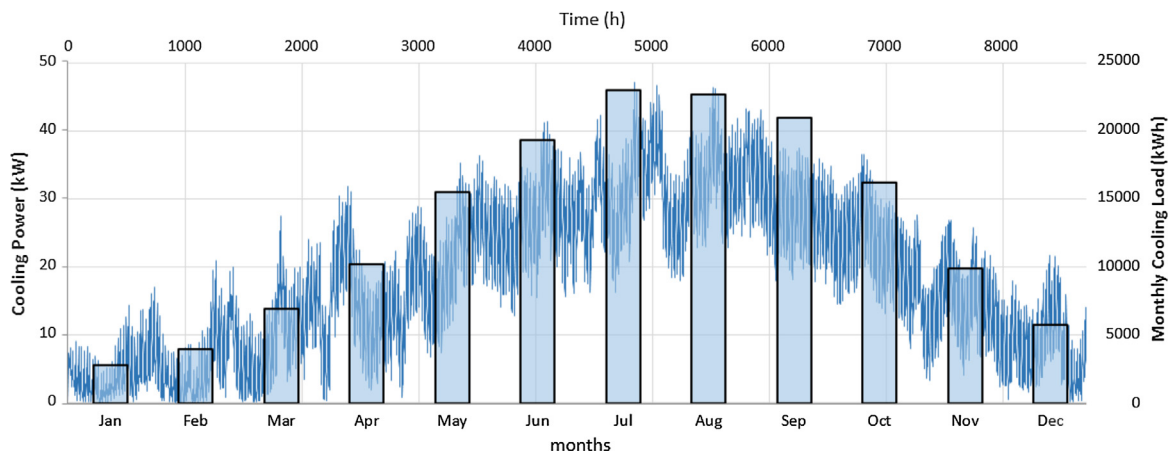


Fig. 9. Building cooling load.

**Table 7**  
Building cooling load.

Peak Load		Annual Load			
Sensible Load	kW	35.00	Sensible Load	kWh	115,338
Latent Load	kW	16.84	Latent Load	kWh	41,223
Total Load	kW	47.31	Total Load	kWh	156,561

the configuration *PTC-2sABS*. Because of the lower efficiency of the single-stage chiller, a larger cooling capacity with a larger storage tank are required to meet the cooling demand. Moreover, the collector aperture area is significantly higher than the *PTC* case (+72.5%),

although *ETCs* can exploit the global incident radiation (including the diffuse component).

### 3. Case study and simulation results

#### 3.1. Building and compound results

The compound is supposed to be located in the Riyadh area (Saudi Arabia). In this region, the climate is warm and dry, with humidity levels very low all year long, as shown in Fig. 7. The ambient temperature shows both daily and seasonal remarkable excursions between maximum and minimum. The air moisture is very low: in the summer

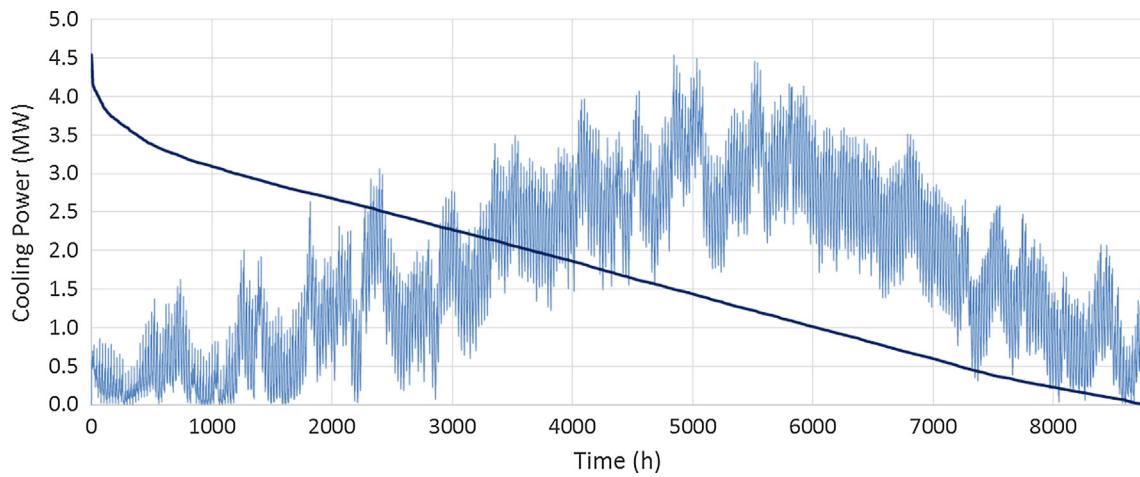


Fig. 10. Cumulated cooling load.

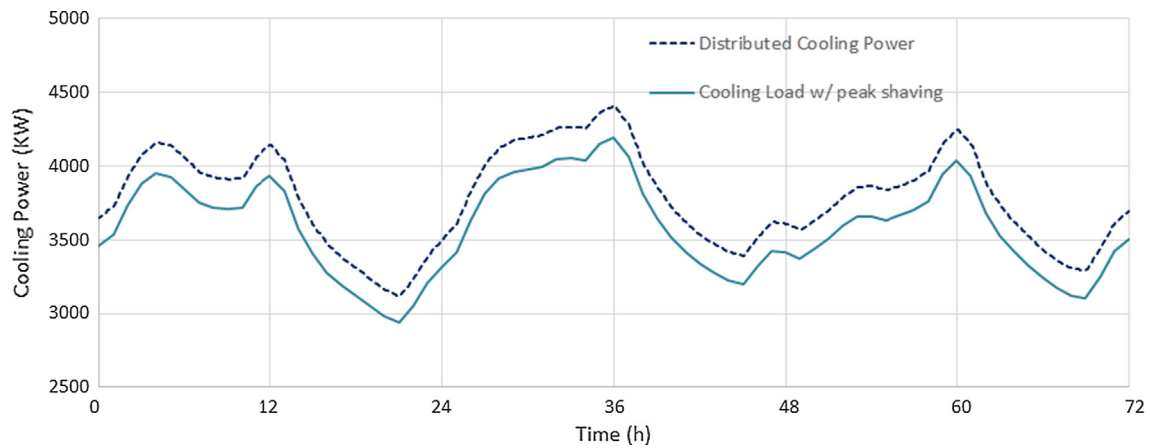


Fig. 11. District network simulation results.

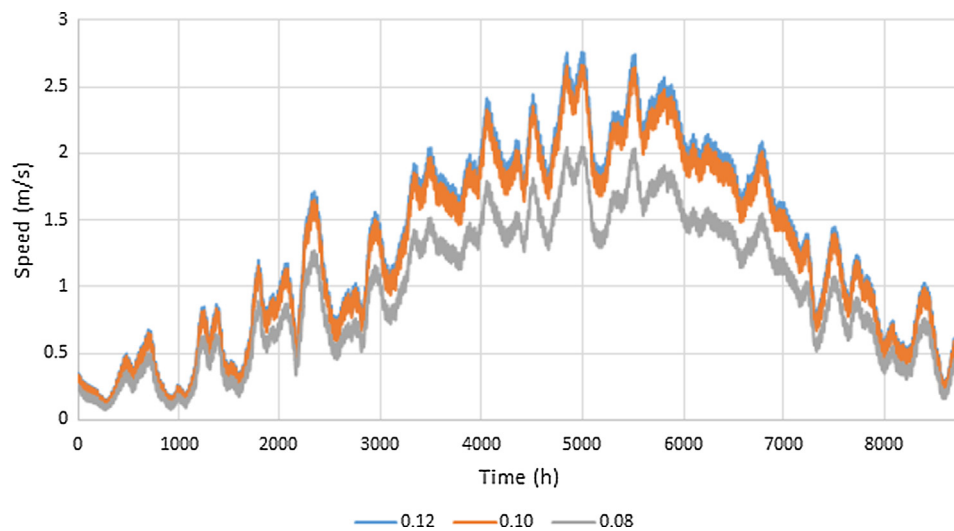


Fig. 12. Water speed in different branches.

period, the relative humidity fluctuates around 20%. This leads to a slight diffusion of the available solar radiation allowing concentrated solar devices to operate efficiently. In Fig. 8 *GHI* and *DNI* are compared: on annual basis they are respectively 2217 kWh/m<sup>2</sup> and 2296 kWh/m<sup>2</sup>.

Starting from the model presented in the Section 2.1, a dynamic simulation of the building thermal behavior was carried out on hourly

basis over 1-year period and the results are reported in Fig. 9, where the monthly cooling demand is superimposed to the instantaneous cooling load. The bars show the cooling load variation during the seasons, whilst the fluctuations show the daily trend influenced by solar radiation and ambient temperature. Peak and annual values are summarized in Table 7. The annual building cooling load resulted 156,561 kWh with



**Table 8**  
Cooling plant performance.

PTC + 2sABS			ETC + ABS		
Cooling load	MWh	16,265	Cooling load	MWh	16,265
Solar energy (based on DNI)	MWh	20,741	Solar energy (based on GHI)	MWh	34,590
PTC Collected heat	MWh	12,612	ETC Collected heat	MWh	20,432
2s Absorption chiller production	MWh	11,438	Absorption chiller production	MWh	11,402
Auxiliary chiller production	MWh	4774	Auxiliary chiller production	MWh	4958
Solar Fraction		0.7	Solar Fraction		0.7

annual demand is 36,381 kWh. The total electricity consumption for the district network pumping stations is 145,525 kWh.

### 3.3. Cooling plant

The annual yield of the two plant configurations is shown in Table 8. The solar fraction is 0.70 for both cases. In spite of a similar absorption chiller cooling production, the required collected heat is significantly higher for ETCs because of the lower efficiency of the single-stage chiller (0.78 vs. 1.36).

Fig. 13 shows the monthly simulation results for the PTC-2sABS case. The difference between the solar energy based on DNI (yellow<sup>1</sup> bars) and the collected heat (red bars) indicates the efficiency of the

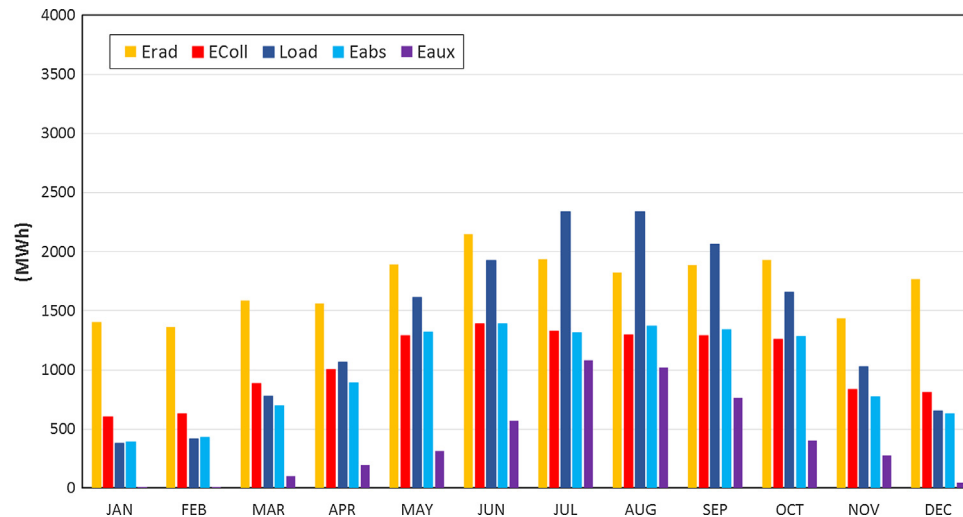


Fig. 13. PTC + 2sABS monthly results.

a peak load of 47.31 kW. The sensible part of the cooling load covers about two-thirds of the total load; the low impact of the latent load is due to the dry climate.

### 3.2. District cooling network

The cooling load was assumed similar for all 96 villas; nevertheless, because of the non-simultaneity of the peak loads, the demand of the whole compound was shaved: the resulting cumulative load is reported in Fig. 10 with the duration curve. The non-simultaneity of the loads is considered with a normal distribution that redistributes 10% of the compound cooling load in the previous and subsequent hours.

The simulation of the district cooling network was carried out over a 1-year period with a time-step of 0.125 h to ensure a high resolution of the results. The computed thermal losses account for approximately 8.2%. Fig. 11 shows a detail of 3-day simulation results: the reported curves indicate the cumulative cooling load corresponding to the 96 villas (with peak shaving due to the non-simultaneity) and the distributed cooling power including piping losses.

The water velocity in the branches of the network with different diameter is shown in Fig. 12. As previously stated, the flow rate is regulated in order to keep constant the temperature levels in the network. It can be seen that the maximum speed is lower than 2.8 m/s also in the peak load periods.

Major losses have been evaluated according to the Darcy equation using a quasi-static approach; only linear losses were considered. For each time-step, the losses were computed for each branch of the network considering the actual water velocity and the pipe characteristics.

Starting from the energy loss calculation, the power of the pumps in the district cooling network was assessed. For each sub-district delivering chilled water to 24 buildings, the peak power is 20 kW and the

solar field, including the tracking system. The cyan and purple bars show the cooling production of absorption and electric chiller respectively; the contribution of the auxiliary cooler is higher than 35% from July to September.

Fig. 14 shows in detail the simulation results related to a 72-h period in summer (left) and winter (right), when the cumulative cooling load is around 2200 kW and 200 kW, respectively. Looking at the solar field operation, in the summer mornings PTCs collect energy to charge the hot tank and to feed the absorption chiller. In the afternoon the 2sABS shows an intermittent operation, because the hot tank control system switches off the pump when the upper temperature limit is achieved (as indicated by the bottom tank temperature reaching the level at the top). Furthermore, the chart shows the important role of the hot storage: the absorption chiller operates also nighttime, even if at partial load because of the decreasing hot water temperature. The auxiliary chiller switches on for a very short time when the temperature in the cold storage tank exceeds the upper limit (10 °C).

During the winter days, the absorption chiller switches on only intermittently, due to the very low cooling demand, and the auxiliary chiller never operates.

The simulation results of the single-stage absorption chiller powered by the ETC field show a different behavior (Figs. 15 and 16). The amount of solar energy (yellow bars in Fig. 15, based on GHI) exploited as source for the district cooling system is 67% higher than the PTC case, because of the lower collector and chiller efficiencies. In the 3-day summer period reported in Fig. 16, the single-stage absorption chiller operates only daytime, whilst during the night the auxiliary unit must

<sup>1</sup> For interpretation of color in Figs. 13 and 15, the reader is referred to the web version of this article.

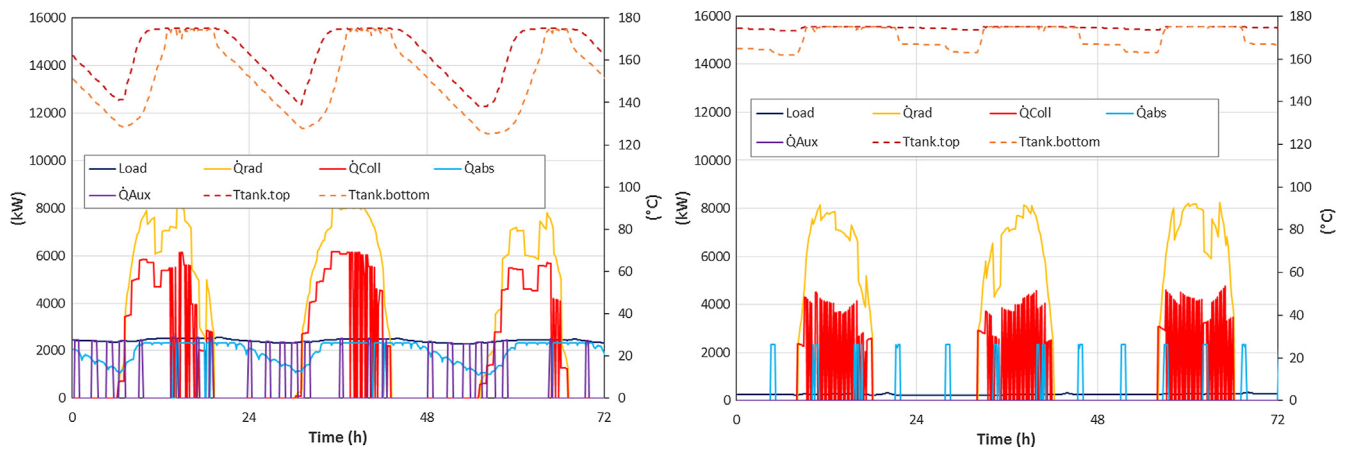


Fig. 14. (PTC + 2sABS) 72-h simulation results: summer (left) and winter (right).

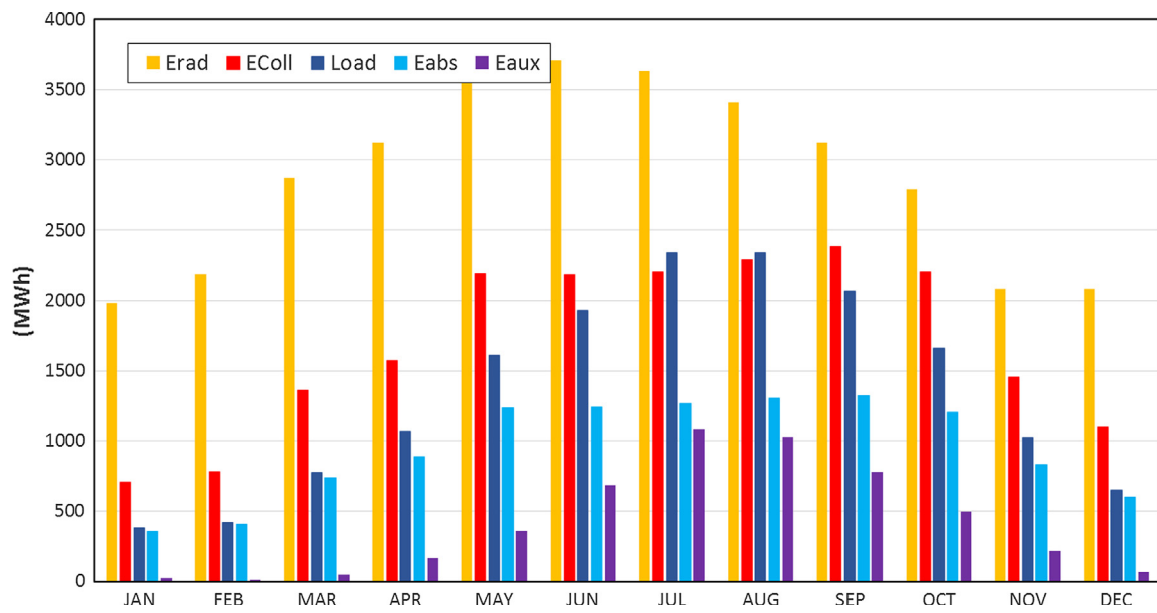


Fig. 15. ETC + ABS monthly results.

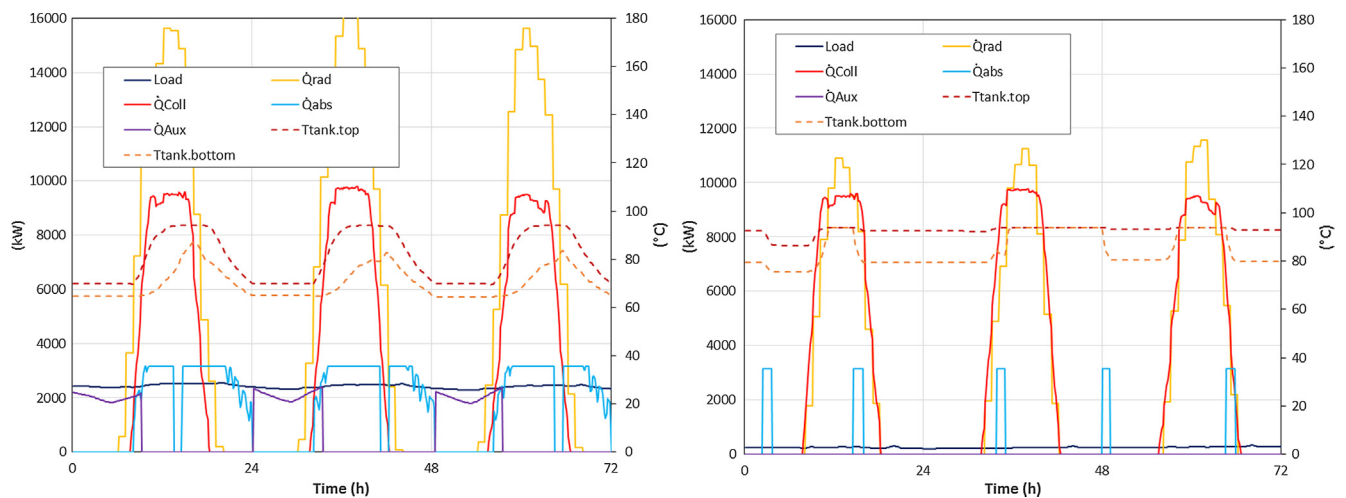


Fig. 16. ETC + ABS 3 day result: summer (left) and winter (right).

switch on to feed the district network, because the hot water temperature in the tank falls under the minimum level (70 °C). The running time of the chillers is influenced by the cooling capacity and the storage

volume calculated in the optimization procedure. The 1sABS has a bigger capacity (3250 vs. 2315 kW) and a lower rated COP (0.723 vs. 1.39) if compared to the 2sABS. This leads to a higher hot water

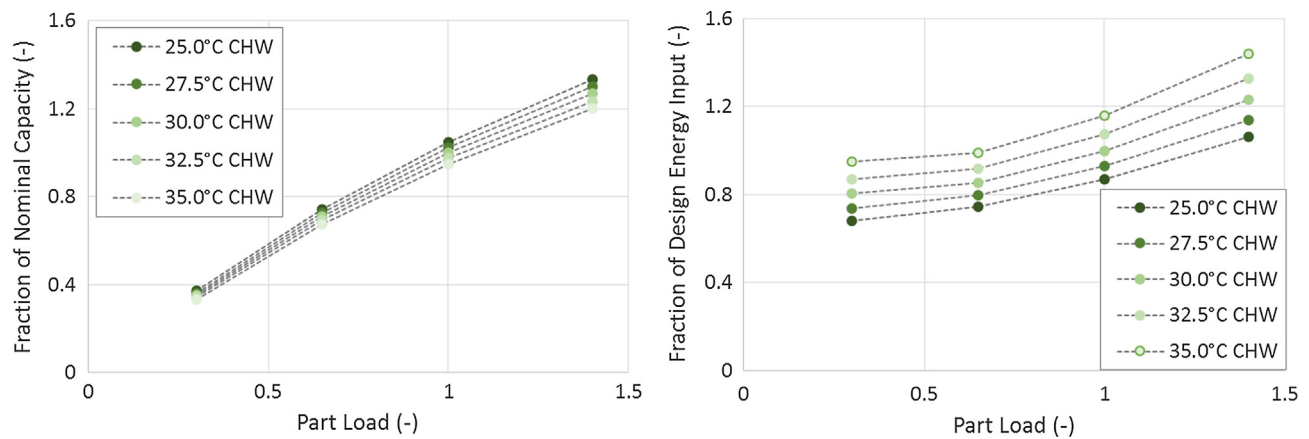


Fig. 17. Compression chiller performance maps.

Table 9

Water-cooled compression chiller technical data.

Compression chiller		
Nominal Capacity <sup>a</sup>	kW	1000
Rated COP <sup>a</sup>	–	5.65
Chilled water	kg/h	170,000
Cooling water	kg/h	203,000

<sup>a</sup> Chilled water (in-out) 12–7 °C; cooling water (in-out) 30–35 °C.

Table 10

Electric energy consumption.

Peak Load			Annual Load		
CC	kW	790	CC	GWh	2.881
1sABS	kW	795	1sABS	GWh	0.878
2sABS	kW	689	2sABS	GWh	0.845

consumption, causing a quicker depletion of the hot tank in spite of the larger capacity (995 vs. 400 m<sup>3</sup>). Moreover, the chiller running time is also related to the performance maps. The 1sABS has a narrower range of driving temperatures (65–95 °C vs. 121–175 °C): the wider temperature dead band of the 2sABS allows for a longer running time (the shut down for minimum temperature in the storage occurs later on).

In winter, the 1sABS switches-on a couple of times per day, and the heat collected by ETCs in the morning is enough to satisfy the daily

Table 11

Primary energy consumption and CO<sub>2</sub> emissions.

Primary energy consumption			Annual CO <sub>2</sub> emission		
CC	TOE	724.33	CC	tonnes/year	2028
1sABS	TOE	220.74	1sABS	tonnes/year	618
2sABS	TOE	212.45	2sABS	tonnes/year	594

Table 12

Budget cost estimation (solar cooling plant).

PTC + 2sABS			ETC + 1sABS		
PTC – solar field	Mio USD	4.337	ETC – solar field	Mio USD	7.800
Hot storage	Mio USD	0.420	Hot storage	Mio USD	0.450
2s Absorption Chiller	Mio USD	1.296	1s Absorption Chiller	Mio USD	1.300
Auxiliary Chiller	Mio USD	0.480	Auxiliary Chiller	Mio USD	0.480
Cold storage	Mio USD	0.090	Cold storage	Mio USD	0.090
Cooling Tower	Mio USD	0.100	Cooling Tower	Mio USD	0.100
TOTAL COST	Mio USD	6.723	TOTAL COST	Mio USD	10.220

load.

Just to compare the investigated solar district cooling configurations and a conventional one, a further district cooling system with identical network and a centralized cooling station based on compression chillers (CC) has been modeled. The cooling station is powered by electricity imported from the grid and includes several chillers with a

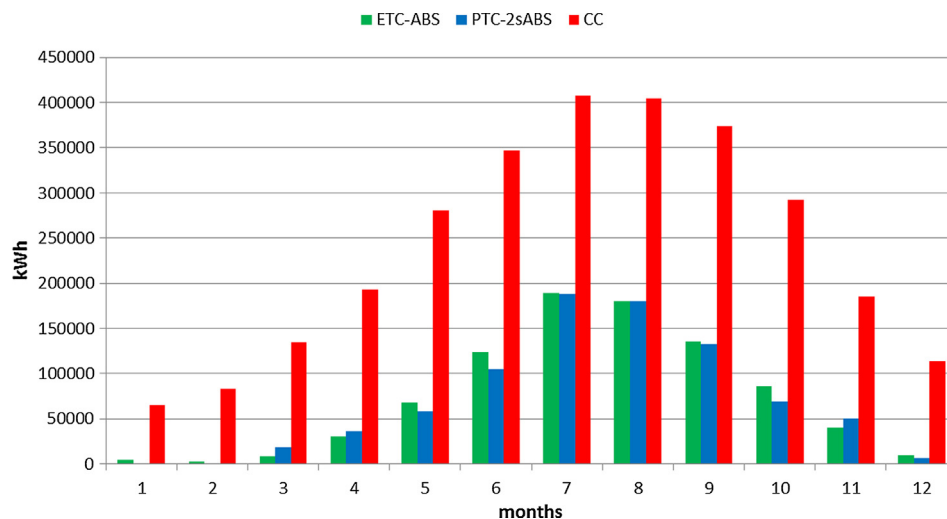


Fig. 18. Monthly electric energy consumption.

**Table 13**  
Budget cost estimation (district network).

DISTRICT NETWORK		
Infrastructure	Mio USD	0.600
Branch	Mio USD	0.347
Heat Interface Unit & Heat Meter	Mio USD	0.254
TOTAL COST	Mio USD	1.201

design capacity of 1 MW each. The compression chiller's Trnsys model is an empirical model similar to the one of the absorption chillers: the COP evaluation is based on the operating maps provided by the manufacturer and presented in Fig. 17, while the main parameters of the compression chiller are shown in Table 9. This CC model was also used to simulate the auxiliary chiller in the 1sABS and 2sABS cases.

Table 10 shows the electricity consumption for the three district cooling plants. The electric consumption of the systems based on absorption chillers includes the auxiliary chiller, the electric equipment and the pumping stations. The three configurations show a similar peak load (in the 1sABS and 2sABS cases the peak power consumption is due to the auxiliary chiller), whilst the annual power consumption is about 70% lower for the solar driven systems (according to the SF). The monthly electricity consumption for the three cooling systems is shown in Fig. 18: in the winter months, the solar cooling systems do not require the auxiliary chiller operation.

Starting from the electrical consumption, the amount of CO<sub>2</sub> emitted for the air conditioning in the three different configurations was estimated. The assessment is carried out using a conversion factor that takes into account the average efficiency of the Saudi power generation systems, as reported in the World Energy Council website [50]. Table 11 shows the primary energy consumption (based on tonnes of oil equivalent) for the required power supply and the related CO<sub>2</sub> production.

#### 4. Economic analysis

The optimization procedure presented in the Section 2 allowed for sizing the main components assuring the budget cost minimization. An estimation of the total budget costs for the two solar district cooling configurations is reported in Tables 12 and 13. The goal of the present analysis is not providing a cost evaluation for a specific application: a number of details (including construction works, design and labor costs, consumables, maintenance, etc.) should be evaluated for a real business plan. The present study aims to compare only the costs that directly depend on the size determined by the optimization algorithm. The values reported in Table 11 are calculated according to the unit costs shown in Table 2 and refer to budget costs provided by market operators and manufacturers. The costs of the district network (Table 13) were estimated using published data [48,49,51]. The cost of the auxiliary chiller is the same for both configurations, as it is designed to cover the peak cooling load in the event of a system failure. The resulting costs for the chiller are similar for the two investigated configurations, whilst the costs of the solar fields are strongly different (+79.8%). This is due to a slight higher unit cost of ETCs (+4%) and the higher efficiency of the two-stage absorption chiller. The network cost accounts for about 15% of the global investment for the case PTC-2sABS.

Such results demonstrate that the solar cooling system based on parabolic troughs and two-stage absorption chiller is attractive and promising for applications in climate conditions similar to Riyadh. Since PTCs can exploit only the beam radiation component, this system is expected to perform well in sites with low humidity levels.

#### 5. Conclusion

In this work two solar district cooling systems including solar field, cooling plant, district network and building load were modeled and simulated for Riyadh climate conditions. The cooling load of a residential compound of 96 single-family detached homes was evaluated and supposed to be covered by a centralized cooling station with a district cooling system supplying chilled water.

The two investigated cooling plants are based respectively on a two-stage absorption chiller driven by Parabolic Trough Collectors (PTCs) and a single-stage absorption chiller driven by Evacuated Tube Collectors (ETCs). An optimization procedure has been developed to determine the size of all main components assuring the cost minimization and an annual solar fraction of 0.7. Transient simulations over 1-year period have been carried out on the two investigated plant configurations to evaluate the energy performance under variable operating conditions. This simulation procedure allowed to predict the annual operation of the solar cooling systems with high level of accuracy. Moreover, the optimization based on the unit costs of the components available on the market permitted a comparison both in terms of efficiency and investment costs. The plant configuration based on PTCs and 2sABS resulted to be significantly more cost effective (−30% of primary costs, including the district network) than the single stage absorption chiller solution for the considered location (Riyadh). This result is due to the higher efficiency of the two-stage absorption chiller (COP 1.39 vs. 0.723, at design conditions) and the high level of direct normal irradiation (2296 kWh/m<sup>2</sup>) available for the concentrated solar devices (PTCs). The results presented in this study can be generalized as a guideline for the design of solar district cooling systems in similar site locations (with high levels of beam solar radiation and dry climate). Furthermore, the paper reports an estimation of the primary energy savings and greenhouse gas emission reduction with respect to a conventional district cooling system based on compression chillers: the solar district cooling system for 96 detached homes with solar fraction 0.7 allows to reduce primary energy consumption and CO<sub>2</sub> emissions by about 500 TOE and 1400 tonnes per year respectively.

#### References

- [1] Morvaj B, Evins R, Carmeliet J. Optimising urban energy systems: simultaneous system sizing, operation and district heating network layout. *Energy* 2016;116:619–36.
- [2] Casisi M, Pinamonti P, Reini M. Optimal lay-out and operation of combined heat & power (CHP) distributed generation systems. *Energy* 2009;34:2175–83.
- [3] Oppelt T, Urbaneck T, Gross U, Platzer B. Dynamic thermo-hydraulic model of district cooling networks. *Appl Therm Eng* 2016;102:336–45.
- [4] Wang H, Wang H, Zhou H, Zhu T. Modeling and optimization for hydraulic performance design in multi-source district heating with fluctuating renewables. *Energy Convers Manage* 2018;156:113–29.
- [5] Rezaie B, Rose MA. District heating and cooling: review of technology and potential enhancements. *Appl Energy* 2012;93:2–10.
- [6] Ameri M, Besharati Z. Optimal design and operation of district heating and cooling networks with CCHP systems in a residential complex. *Energy Build* 2016;110:135–48.
- [7] Romanchenko D, Kensby J, Odenberger M, Johnsson F. Thermal energy storage in district heating: centralised storage vs. storage in thermal inertia of buildings. *Energy Convers Manage* 2018;162:26–38.
- [8] Olsthoorn D, Haghighat F, Mirzaei PA. Integration of storage and renewable energy into district heating systems: a review of modelling and optimization. *Sol Energy* 2016;136:49–64.
- [9] Elci M, Oliva A, Herkel S, Klein K, Ripka A. Grid-interactivity of a solar combined heat and power district heating system. *Energy Procedia* 2015;70:560–7.
- [10] Schmidt T, Mangold D, Müller-Steinhagen H. Central solar heating plants with seasonal storage in Germany. *Sol Energy* 2004;76:165–74.
- [11] Powell KM, Cole WJ, Ekarika UF, Edgar TF. Optimal chiller loading in a district cooling system with thermal energy storage. *Energy* 2013;50:445–53.
- [12] Gang W, Wang S, Xiao F, Gao D. Performance assessment of district cooling system coupled with different energy technologies in subtropical area. *Energy Procedia* 2015;75:1235–41.
- [13] Liew PY, Theo WL, Wan Alwi SR, Lim JS, Manam ZA, Klemes JJ, et al. Total Site Heat Integration planning and design for industrial, urban and renewable systems. *Renew Sustain Energy Rev* 2017;68:964–85.
- [14] Ozgener L. Coefficient of performance (COP) analysis of geothermal district heating systems (GDHS): Salihli GDHS case study. *Renew Sustain Energy Rev*



- 2012;16:1330–4.
- [15] Eriksson M, Vamling L. Future use of heat pumps in Swedish district heating systems: short- and long-term impact of policy instruments and planned investments. *Appl Energy* 2007;84:1240–57.
  - [16] Lund H, Möller B, Mathiesen BV, Dyrelund A. The role of district heating in future renewable energy systems. *Energy* 2010;35:1381–90.
  - [17] Trier D. Towards solar district heating with more than 70% solar fraction. *Energy Procedia* 2015;70:580–6.
  - [18] Chasapis D, Drosou V, Papamechael I, Aidonis A, Blanchard R. Monitoring and operational results of a hybrid solar-biomass heating system. *Renew Energy* 2008;33:1759–67.
  - [19] Carpaneto E, Lazzeroni P, Repetto M. Optimal integration of solar energy in a district heating network. *Renew Energy* 2015;75:714–21.
  - [20] Zeng J, Han J, Zhang G. Diameter optimization of district heating and cooling piping network based on hourly load. *Appl Therm Eng* 2016;107:750–7.
  - [21] Sameti M, Haghighat F. Optimization approaches in district heating and cooling thermal network. *Energy Build* 2017;140:121–30.
  - [22] van der Heijde B, Fuchs M, Tugores CR, Schweiger G, Sartor K, Basciotti D, et al. Dynamic equation-based thermo-hydraulic pipe model for district heating and cooling systems. *Energy Convers Manage* 2017;151:158–69.
  - [23] Chan ALS, Hanby VI, Chow TT. Optimization of distribution piping network in district cooling system using genetic algorithm with local search. *Energy Convers Manage* 2007;48(10):2622–9.
  - [24] Chorowski M, Rogala Z, Pyrka P. System options for cooling of buildings making use of district heating heat. *Int J Refrig* 2016;70:183–95.
  - [25] Arabkoohsar A, Andresen GB. Supporting district heating and cooling networks with a bifunctional solar assisted absorption chiller. *Energy Convers Manage* 2017;148:184–96.
  - [26] Lake A, Rezaie B, Beyerlein S. Review of district heating and cooling systems for a sustainable future. *Renew Sustain Energy Rev* 2017;67:417–25.
  - [27] Horn P, Hauer S, Judex F, Kreulitsch D, Selke T. Solar hybrid heating & cooling systems on district level-The Austrian Project CiQuSo. *Energy Procedia* 2016;91:980–8.
  - [28] Gang W, Wang S, Xiao F, Gao D. District cooling systems: technology integration, system optimization, challenges and opportunities for applications. *Renew Sustain Energy Rev* 2016;53:253–64.
  - [29] Marugán-Cruz C, Sánchez-Delgado S, Rodríguez-Sánchez MR, Venegas M, Santana D. District cooling network connected to a solar power tower. *Appl Therm Eng* 2015;79:174–83.
  - [30] Perdichizzi A, Barigozzi G, Franchini G, Ravelli S. Performance prediction of a CSP plant integrated with cooling production. *Energy Procedia* 2015;75:436–43.
  - [31] Zhai XQ, Qu M, Li Y, Wang RZ. A review for research and new design options of solar absorption cooling systems. *Renew Sustain Energy Rev* 2011;15:4416–23.
  - [32] Atmaca I, Yigit A. Simulation of solar-powered absorption cooling system. *Renew Energy* 2003;28:1277–93.
  - [33] Florides GA, Kalogirou SA, Tassou SA, Wrobel LC. Modelling, simulation and warming impact assessment of a domestic-size absorption solar cooling system. *Appl Therm Eng* 2002;22:1313–25.
  - [34] Assilzadeh F, Kalogirou SA, Ali Y, Sopian K. Simulation and optimization of a LiBr solar absorption cooling system with evacuated tube collectors. *Renew Energy* 2005;30:1143–59.
  - [35] Sokhansefat T, Mohammadi D, Kasaeian A, Mahmoudi AR. Simulation and parametric study of a 5-ton solar absorption cooling system in Tehran. *Energy Convers Manage* 2017;148:339–51.
  - [36] Figueredo GR, Bourouis M, Coronas A. Thermodynamic modelling of a two-stage absorption chiller driven at two-temperature levels. *Appl Therm Eng* 2008;28:211–7.
  - [37] Mazloumi M, Naghashzadegan M, Javaherdeh K. Simulation of solar lithium bromide–water absorption cooling system with parabolic trough collector. *Energy Convers Manage* 2008;49:2820–32.
  - [38] El Fadar A, Mimet A, Pérez-García M. Modelling and performance study of a continuous adsorption refrigeration system driven by parabolic trough solar collector. *Sol Energy* 2009;83:850–61.
  - [39] Brumana G, Franchini G. Solar-powered air conditioning for buildings in hot climates: desiccant evaporative cooling vs. absorption chiller-based systems. *Energy Procedia* 2016;101:288–96.
  - [40] Nurzia G, Franchini G, Perdichizzi A. Combined solar heating and cooling systems: simulation and design optimization, ASME Paper ES2008-54127, Jacksonville, FL, USA: ASME International Solar Energy Division; August 10–14, 2008.
  - [41] Hang Y, Du L, Qu M, Peeta S. Multi-objective optimization of integrated solar absorption cooling and heating systems for medium-sized office buildings. *Renew Energy* 2013;52:67–78.
  - [42] Calise F, d'Accadia MD, Vanoli L. Thermoeconomic optimization of solar heating and cooling systems. *Energy Convers Manage* 2011;52(2):1562–73.
  - [43] Kirgat GS, Surde AN. Review of hooke and jeeves direct search solution method analysis applicable to mechanical design engineering. *Int J Innov Eng Res Technol (IJIERT)* 2014;1(2):1–14.
  - [44] Remund J, et al. *Meteonorm handbook, part II: theory*. Bern, Switzerland: Meteotest; 2000.
  - [45] Halldor K, Böhm B. Advanced and traditional pipe systems: optimum design of distribution and service pipes. *Euroheat and Power* 3.IV/2006; 2006: 34–42.
  - [46] ASHRAE. *Fundamentals Handbook*; edition S. I. American society of heating, refrigerating and air-conditioning engineers. Inc; 1997. 33.2.
  - [47] Schmidt T, Miedaner O. Design Optimization with GenOpt®, Building Energy Simulation User News 21 (Sep./Oct. 2000).
  - [48] Wetter M. Solar district heating guidelines. *Solites* 2012.
  - [49] IEA-ETSAP, I. R. E. N. A., Thermal energy storage: Technology brief e17; 2013.
  - [50] <https://www.worldenergy.org/data/efficiency-indicators/>.
  - [51] Davies G, Woods P. The potential and cost of district heating network, 2009 Pöyry Energy (Oxford).